Chapter

Uncertainty Quantification in Electromagnetic Computation

Geoffrey Lossa and Olivier Deblecker

Abstract

In this work, uncertainty quantification is integrated to assess the sensitivity of a finite element (FE)-based numerical model to uncertainties in its input parameters. We compute the sensitivity of wound inductors' RL parameters extracted from the FE method with respect to geometric and material uncertainties across a wide range of frequencies (from DC to 1 MHz). To that end, we propose a 2D modeling of geometric uncertainties associated with conductors' positions in the winding window, and we compute the *Sobol* indices associated with a polynomial chaos expansion-based surrogate model of the uncertain FE model using Bayesian inference techniques.

Keywords: finite element, homogenization technique, uncertainty quantification, inference technique, polynomial chaos expansion, wound inductors

1. Introduction

Numerical models of a physical system almost always depend on uncertain parameters. For instance, wound inductors are characterized by material uncertainties (material properties that are not accurately known) and geometric uncertainties (2D positions of conductors in the winding window, as depicted in **Figure 1**, air-gap dimensions, etc.). Correct modeling of such uncertainties, as well as a good understanding of the sensitivity of physical quantities with respect to uncertainties, is fundamental for ensuring an optimal design of the component.

The finite element (FE) method can be employed to capture these uncertainties in RLC models using a Monte Carlo (MC) simulation approach [1]. However, performing a sensitivity analysis with such a model is very CPU-intensive. In this work, we develop a stochastic surrogate model of wound inductors based on polynomial chaos expansion (PCE) in order to mitigate this problem. We then compute the *Sobol* indices [2, 3] over a wide range of frequencies (from DC to 1 MHz) to quantify the sensitivity of RL parameters from the PCE surrogate model.

Sensitivity analysis is not limited to determining how the variability of the model is affected by the variability of each random input, but it can also be used to highlight unimportant inputs and thereby help reduce the dimension of the stochastic problem. In general, it can be based on the correlation between input and output parameters (correlation based on measurements), on values of partial derivatives of

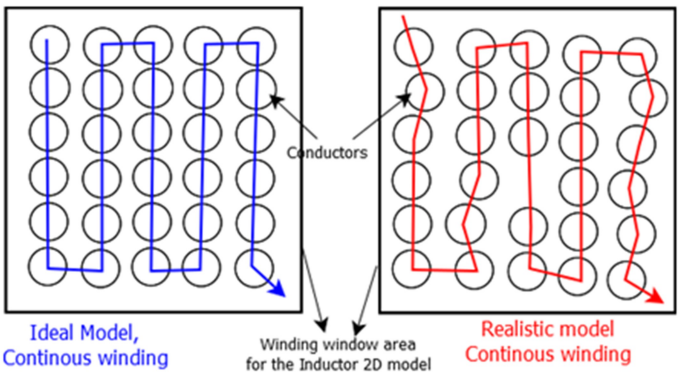

Figure 1.
Illustration of geometric uncertainties in a 2D pattern of a five-layer winding.

the model at a given point (linear method), or even directly on the distribution of the model output. The global sensitivity analysis is based more specifically on the decomposition of the variance of the model response in terms of the contribution of each input parameter or their combinations. This is the case, for example, with the *Sobol* sensitivity indices [2].

2. Methodology

The uncertainties taken into account in this study arise from the random positions of conductors in the winding window and from the material properties of the ferrite core (magnetic permeability $\underline{\mu}_{core}$ and electrical conductivity σ_{core}). The complex form of material properties allows for the natural consideration of electrical and magnetic losses in FE formulations.

Due to the high number of MC iterations with an embedded time-consuming FE-based model, especially with regard to the high number of geometric uncertainties, the reduction in the dimension of the problem is required and is achieved through the transformation of geometrical uncertainties (2D positions of conductors) into material ones (equivalent magnetic reluctivity $\underline{\nu}_{prox}$ related to the proximity effect and equivalent impedance $\underline{Z}_{skin}$ related to the skin effect) via a homogenization technique [4–6].

The overall methodology is built upon a stochastic surrogate model [4] for the computation of RL parameters, in combination with an original algorithm mimicking the manual winding operation [7] in order to model the uncertain positions of conductors in the winding window. It is depicted in **Figure 2**. We compute a PCE surrogate in order to reduce the computation time associated with the FE-based numerical model during calls needed to perform a MC simulation (with a brute FE model). In addition to this, we compute the *Sobol* coefficients from the PCE surrogate, which does not require any additional evaluation of the deterministic model (which is expensive in terms of resources and computation time) once it has been built. This is due to one of the important properties of PCE: that of containing information on its ANOVA (analysis of variance) decomposition.

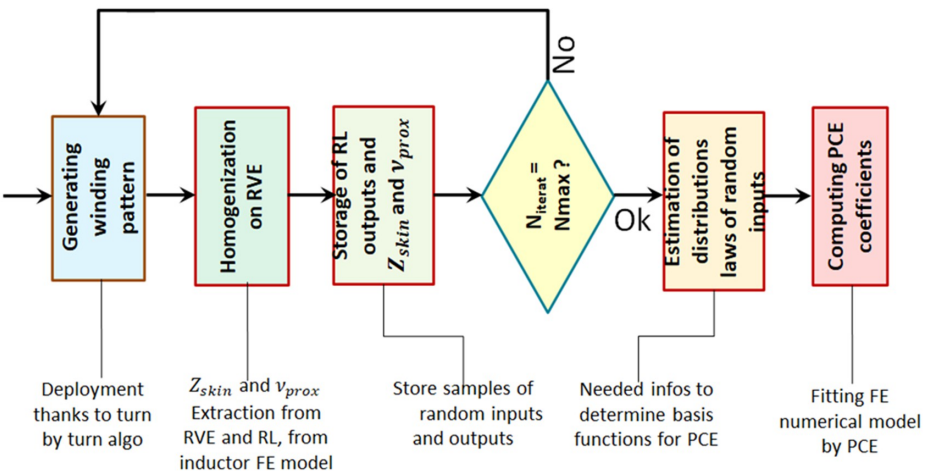

Figure 2.
Process of PCE surrogate construction.

According to this chart, N_{iter} is the number of iterations needed to build the PCE surrogate from distributions of the reduced random input vector. N_{iter} is bounded by N_{max} which is a value linked to the dimension of the random input vector. In our case, without the homogenization process, which allows us to transform geometrical uncertainties into material ones, this dimension can easily reach an order of magnitude close to 100.

A 2D magneto-harmonic formulation with massive conductors and appropriate limit conditions on an optimal representative volume element (RVE) [8] in the winding allows the extraction of the desired equivalent properties (electric conductivity and magnetic reluctivity, for instance). Finally, the dimension of the random input is reduced to seven components, among which we find:

- $X_1 = \mathfrak{Re}(\underline{Z}_{skin})$, image of losses due to skin effect phenomena in the winding;
- $X_2 = \mathfrak{Im}(\underline{Z}_{skin})$, image of the reactive power transmitted by the winding;
- $X_3 = \mathfrak{Re}(\underline{\nu}_{prox})$, image of the energy associated with the proximity effect in the winding;
- $X_4 = \mathfrak{Im}(\underline{\nu}_{prox})$, image of losses linked to the proximity effect between conductors;
- $X_5 = \mathfrak{Re}(\underline{\nu}_{core})$, image of the magnetic energy in the ferrite core;
- $X_6 = \mathfrak{Im}(\underline{\nu}_{core})$, image of the ferrite core losses;
- $X_7 = \sigma_{core}$, image of losses due to the eddy current in the ferrite core. It is a scalar depending on the imaginary part of the electric permittivity $\underline{\epsilon}_{core}$.

For the computation of the PCE surrogate model, we need to know the distribution law of the obtained reduced random input vector. This problem is

associated with the inverse problem, where unknown parameters (related to distributions) are estimated based on experimental data, which are indirectly associated with these parameters through a computational model. This problem can be solved using Bayesian methods, particularly the Bayesian inference technique [9]. This technique consists of the backward propagation of information about observations in order to extract the distribution of the model inputs. For instance, in statistical inference, one considers that the data consist of independent realizations of an underlying random vector and an assumption on the shape of the probability density function PDF (e.g., Weibull, Gaussian, log-normal, etc.). The tools used here are based on UQLab, which is a framework that can be plugged into MATLAB to perform uncertainty quantification [10].

The *Sobol* decomposition of a truncated PCE can be established analytically in terms of increasing orders as follows.

$$\begin{aligned}\mathcal{M}_p(X) = a_0 &+ \sum_{i=1}^{M}\sum_{\alpha\in\mathcal{I}_i} a_\alpha \Psi_\alpha(X_i) \\ &+ \sum_{1\le i_1<i_2\le M}^{M}\sum_{\alpha\in\mathcal{I}_{i_1,\,i_2}} a_\alpha \Psi_\alpha(X_{i_1},X_{i_2}) + \cdots \\ &+ \sum_{1\le i_1<\cdots<i_s\le M}^{M}\sum_{\alpha\in\mathcal{I}_{i_1,\cdots,\,i_s}} a_\alpha \Psi_\alpha(X_{i_1},\cdots,X_{i_s}) + \cdots \\ &+ \sum_{\alpha\in\mathcal{I}_{1,\cdots,\,M}} a_\alpha \Psi_\alpha(X) \end{aligned} \tag{1}$$

where the set $\mathcal{I}_{i_1,\cdots,i_s}$ corresponds to Ψ_α polynomials depending on all parameters $\{X_{i_1},\cdots,X_{i_s}\}$ and nothing but them. It is defined as:

$$\begin{aligned}\mathcal{I}_{i_1,\cdots,i_s} = \{&\alpha\in\mathbb{N}^M :\ 0\le|\alpha|\le p, \\ &k\in\{1,\cdots,M\}/\{i_1,\cdots,i_s\},\ \alpha_k = 0\}\end{aligned} \tag{2}$$

One can highlight the dependence of each multivariate polynomial on each subset of input parameters for clarity. This allows us to deduce the variance of the decomposition in the following way:

$$\mathbb{V}[\mathrm{M}(X)] \equiv D_p = \sum_{i=1}^{M} D_i + \sum_{1\le i<j\le M} D_{ij} + \cdots + D_{1,\cdots,M} \tag{3}$$

where $D_{i_1,\cdots,i_s}$ refer to partial variances and are defined as:

$$D_{i_1,\cdots,i_s} = \mathbb{V}[\mathcal{M}_{i_1,\cdots,i_s}(X_{i_1},\cdots,X_{i_s})],\ s = 1,\cdots,M \tag{4}$$

From these last expressions, it is possible to define the sensitivity index $\mathcal{S}^p_{i_1,\cdots,i_s}$ of the model response for the subset of random input variables $\{X_{i_1},\cdots,X_{i_s}\}$ as:

$$\mathcal{S}^p_{i_1,\cdots,i_s} = \frac{D_{i_1,\cdots,i_s}}{D_p} = \frac{1}{D_p}\sum_{\alpha\in\mathcal{I}_{i_1,\cdots,i_s}} a_\alpha^2 \tag{5}$$

In addition, total sensitivity indices, also based on PCE, can be defined to assess the total effect of an input parameter as follows:

$$\mathcal{S}_i^{T,p} \sum_{i_1,\cdots,i_s \in \mathcal{I}_i^+} \frac{D_{i_1,\cdots,i_s}}{D_p} \frac{1}{D_p} \sum_{\alpha \in \mathcal{I}_i^+} a_\alpha^2 \tag{6}$$

where $\mathcal{I}_i^+$ indicates the set of all indices involving the i^{th} input parameter with a non-zero index, that is:

$$\mathcal{I}_i^+ \equiv \left\{ \alpha \in \mathbb{N}^M : \ 0 \le |\alpha| \le p, \ \alpha_i \ne 0 \right\} \tag{7}$$

2.1. Algorithm for generating realistic 2D winding patterns for stochastic FE modeling of wound inductors

According to this algorithm, conductors are deployed turn after turn. It aims to emulate the manual process as it would be carried out by an operator (**Figure 3**). The algorithm includes the following actions.

- The first layer conductors are the ones that are deployed first. For these, we only observe uncertainties δ_y according to their vertical axis because they are placed against the magnetic core's central column.

- Conductors of the second and subsequent layers, except for their last conductors, are deployed to intersect with conductors of previous layers while maintaining two points of tangency with the latter.

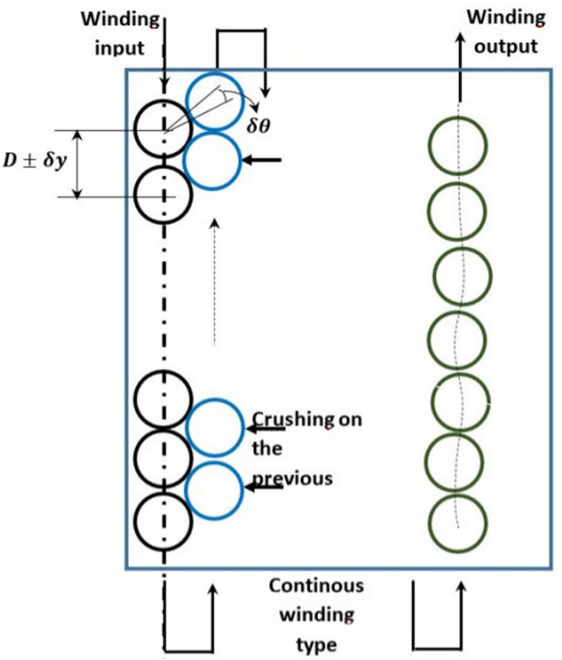

Figure 3.
Principle of the simulation of winding construction.

- In case there is an overlap between two conductors, it is necessary to redeploy the conductor corresponding to the turn being deployed in order to maintain two points of tangency: one with the conductor of the same layer as itself.

- The last conductors of the second and subsequent layers are positioned to present an uncertainty of δ_θ angle and a point of tangency with their corresponding conductors in the previous layer.

- In the event of an overlap with the conductor of the same layer, a redeployment is carried out to contract two points of tangency (with the conductor of the same layer and its corresponding conductor from the previous layer).

This original method of deploying the conductors in the winding window can be used to support the propagation of geometric uncertainties in a deterministic model, such as the FE method embedded into a MC simulation. To validate this approach, let us analyze the influence of geometric uncertainties related to the positions of conductors in the extraction of RLC parameters of a wound inductor made of an Mnzn type ferrite core. Its magnetic core, without an air-gap, is considered ideal – that is, without electrical and magnetic losses (a relative magnetic permeability of 1,000 and 0 electric conductivity are considered). For this analysis, a 2D model is sufficient due to the axisymmetric characteristic of the geometry (see **Figure 4**). The copper conductors have a diameter of 0.315 mm. They are deployed in the winding window using our developed algorithm simulating the winding process.

Results presented in **Figure 5** are from a MC simulation of 390 iterations. According to this figure, one can observe an increasing dispersion of the R parameter due to the appearance of skin and proximity effects with increasing frequency, while the L and C parameters maintain a quasi-constant dispersion over the analysis frequency range and decrease with increasing frequency. In this figure, dispersions

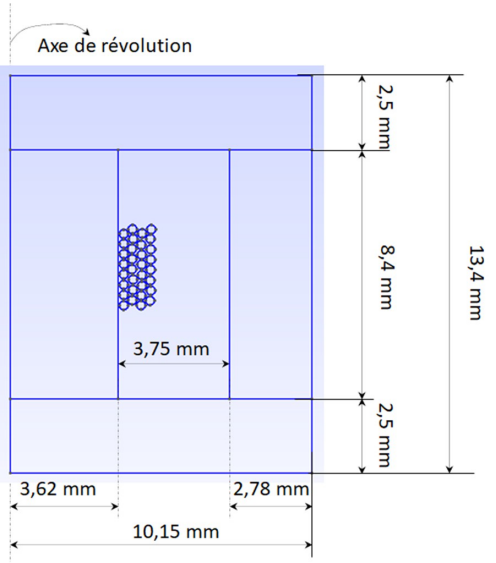

Figure 4.
Geometry taken into account to illustrate the propagation of uncertainties related to the positions of conductors in the winding window.

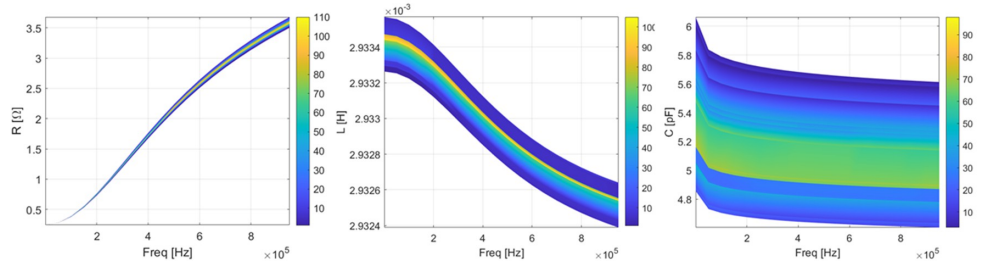

Figure 5.
Evolution of RLC parameters superimposed on their distributions in the form of colored map, as functions of frequency.

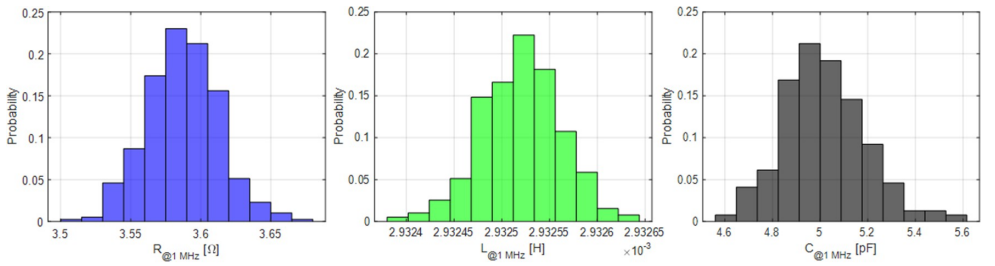

Figure 6.
RLC parameter histograms (with probability densities on the ordinate) taken at 1 MHz.

of different parameters are superimposed in the form of colored maps to their evolutions. Their scale represents the number of realizations of each value associated with each parameter.

The stopping criterion for this MC simulation is based on the convergence of the mean of each parameter of interest. According to this criterion, one can see from **Figure 6** that the number of MC iterations is sufficient. A zoom at 1 MHz on the distributions of RLC parameters can be observed in **Figure 7**. We can observe in the latter normal distributions, which reflect the nature of uncertainties linked to the positions of conductors in the winding window.

3. Case study

In this work, we analyze a typical commercial inductor (MCSCH895-680KU, as illustrated in **Figure 8**). It is made up of a NiZn ferrite core type, with a 44-turn winding distributed over four layers. The first three layers include 12 turns per layer. The conductor diameter is 0.37 mm. According to the manufacturer, this inductor is characterized by a nominal inductance value of 68 μH $\pm$ 10%. The material properties of the ferrite core are modeled using a *Debye* relaxation model along the frequency range of study [11]. In this model, the random aspect is represented by static quantities for which the manufacturer often provides the relative error (20% for magnetic permeability and 10% for electrical conductivity). The dimension of the random input vector (set of geometrical and material uncertainties) of the studied inductor numerical model has been reduced to seven, among which are the real and

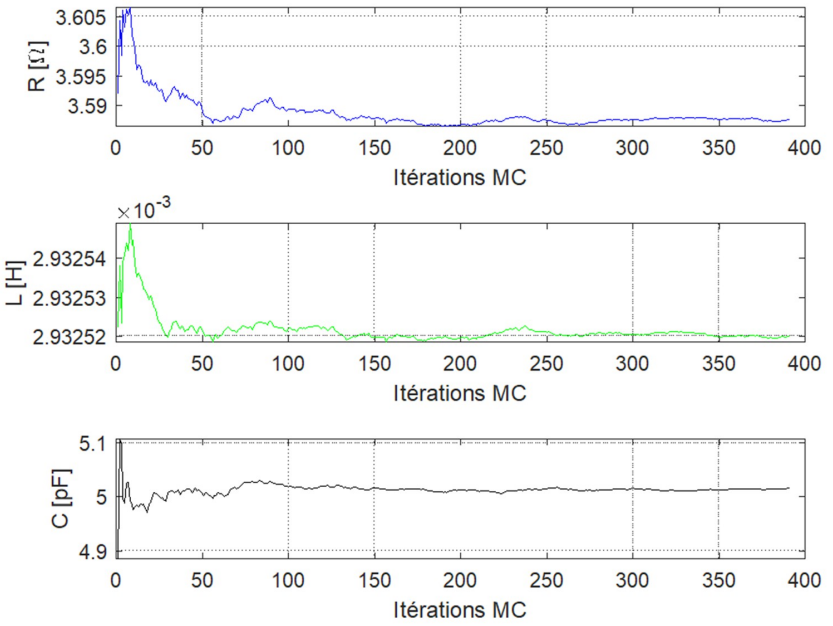

Figure 7.
Evolution of average RLC parameters measured at 1 MHz as a function of the number of MC iterations (stopping criterion).

Figure 8.
Illustration of the analyzed component.

imaginary parts of $\underline{\nu}_{prox}$, $\underline{Z}_{skin}$, and $\underline{\mu}_{core}$ and the ferrite core conductivity σ_{core}. Results of the sensitivity analysis will be presented in the section below.

4. Simulation results

To build the stochastic surrogate model based on PCE (using the least angle regression algorithm implemented in UQLab, see Appendix A), 295 calls of the numerical model were sufficient. In order to transform geometric uncertainties into material ones and to extract *RL* parameters, the homogenization technique has been implemented in GetDP and Gmsh [12] as computation tools for FE formulations. For experimental validation, *RL* parameters were measured across a wide range of

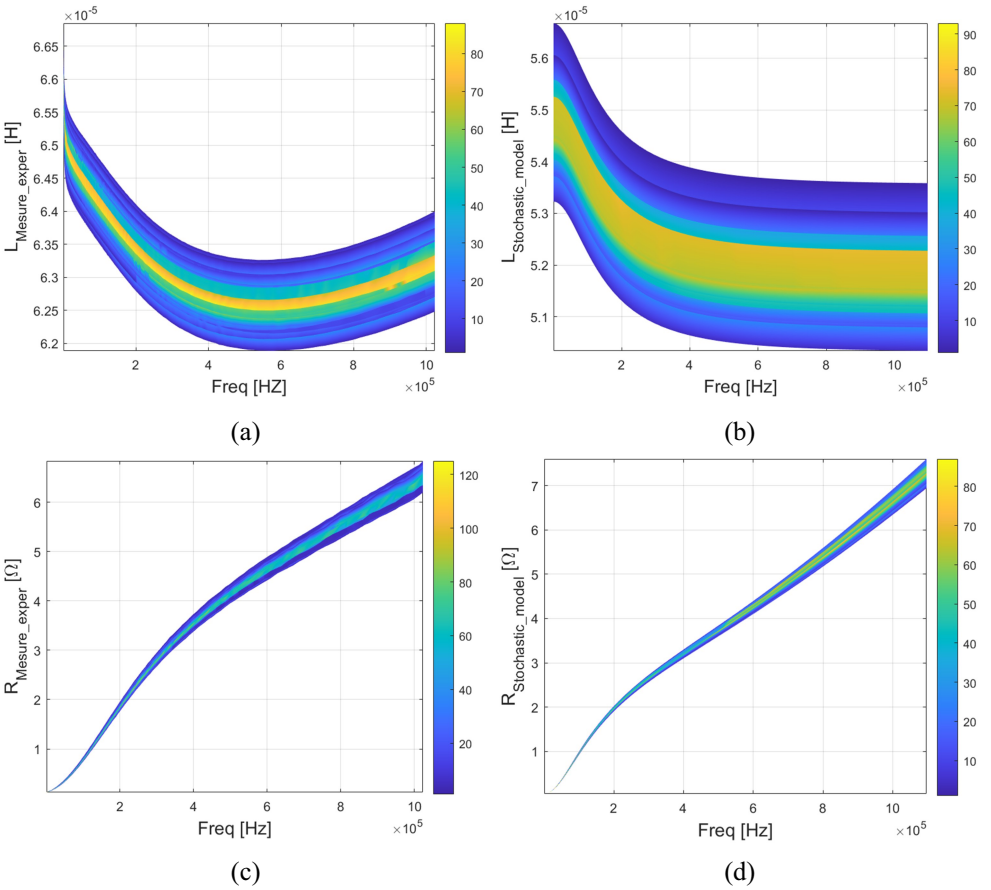

Figure 9.
Evolution of RL parameters superimposed with their distributions in terms of colored maps, experimentally measured on a batch of 299 MCSCH895-680KU inductors (left) and extracted from stochastic surrogate models (right).

frequencies using a Wayne Kerr impedance analyzer [13]. **Figure 9** shows good agreement between the two evolutions of *RL* parameters. One can observe an increasing dispersion with frequency in both evolutions (experimental measurement and simulation), especially in the *R* parameter, due to the occurrence, with increasing frequency, of skin and proximity effects as well as Joule losses in the ferrite core.

Figure 10 presents distributions of RL parameters at 537 kHz and 1 MHz. Regarding the *R* parameter, distributions overlap with increasing frequency due to the increasing dispersion associated with skin and proximity effects. On the other hand, the increasing dispersion is less marked in the case of the *L* parameter. From the order of magnitude of this parameter (less than 0.1 mH) and its low relative error (10% according to data provided by the manufacturer and experimental measurements), we understand why we do not observe any overlap between the distributions associated with the experimental measurements and the stochastic model of this parameter. This parameter exhibits low dispersion over the range of frequencies studied and thus retains a quasi-deterministic

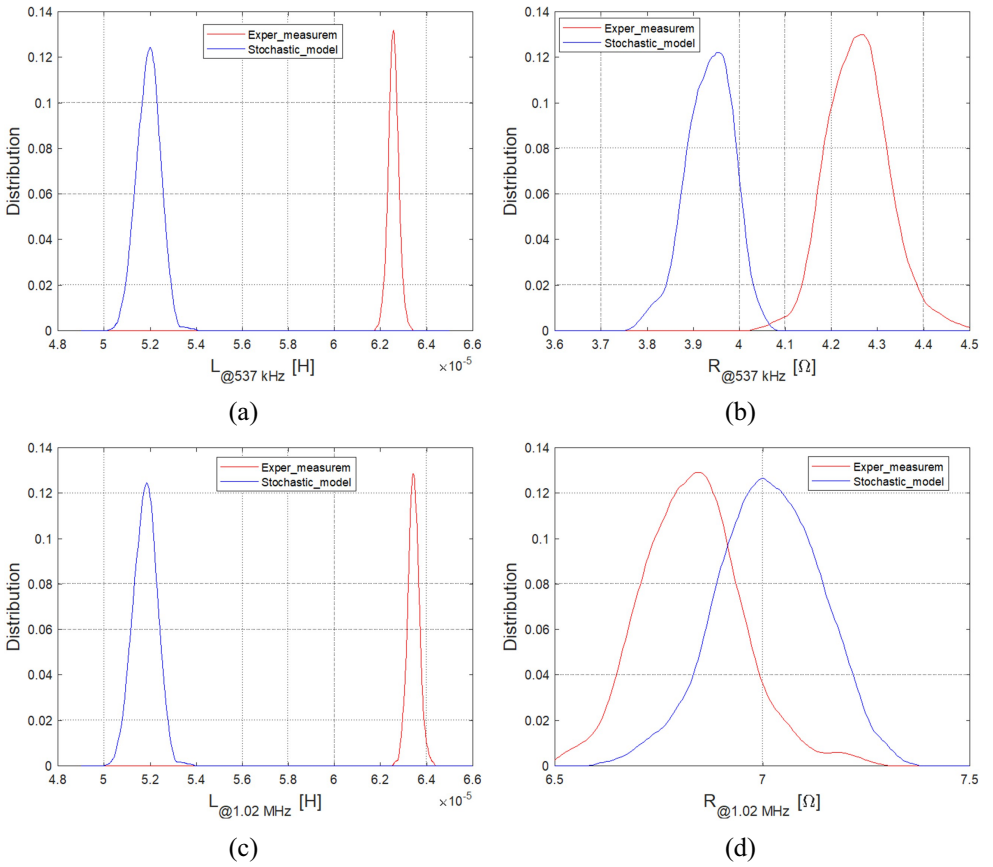

Figure 10.
Comparison between the distributions of RL parameters from experimental measurements and the stochastic model for frequencies 537 kHz (above) and 1.02 MHz (below).

aspect. From such behavior, one should expect low sensitivity to the uncertainties that are taken into account in the stochastic model (as discussed below).

The post-processing of the obtained PCE allowed for sensitivity analysis to be carried out through the computation of *Sobol* indices. The evolution of *Sobol* indices related to each component of the reduced input random vector over a wide range of frequencies is presented in **Figure 11**.

The L parameter seems less influenced by variations in random inputs. This may explain its quasi-deterministic behavior. Only three input variables (X_3, X_4, and X_5) have an influence on this parameter. The dependence with respect to X_5 is obvious because the latter expresses the stored magnetic energy in the inductor, which decreases with frequency. This decrease may be explained by the circumvention of conductors by field lines when the operating frequency increases. On the other hand, the dependence with respect to X_3 and X_4 clearly demonstrates the significant influence of geometrical uncertainties on the L parameter.

Regarding the R parameter, one can observe the influence of several random input variables. This may also justify the strong dispersion of this parameter and the increase in dispersion with frequency. This is linked to the occurrence of several

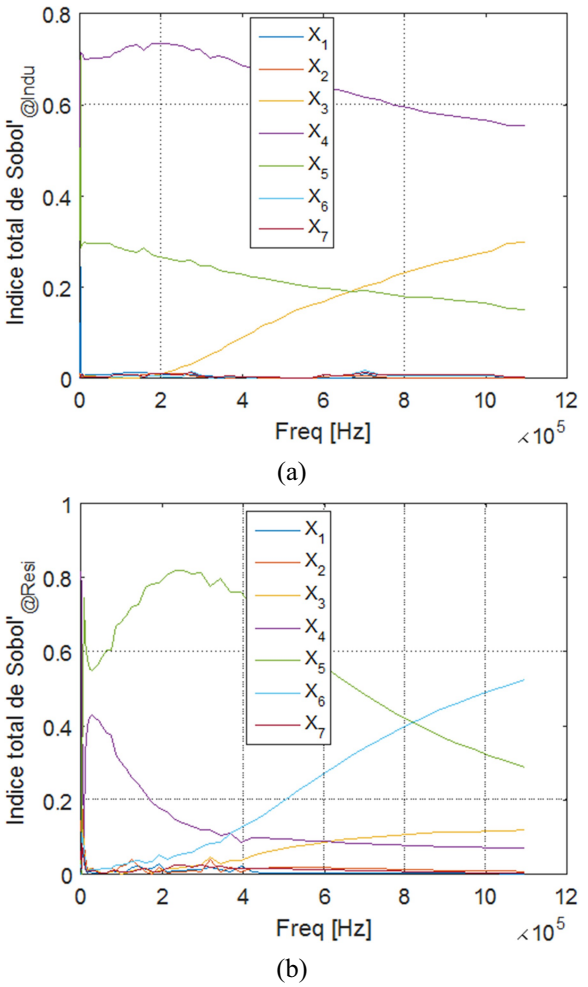

Figure 11.
Total Sobol *indices for stochastic models of* L *(above) and* R *(below).*

phenomena with increasing frequency, including skin and proximity effects through conductors in the winding.

Its dependence on imaginary parts X_2, X_4, and X_6 is obvious since the latter are images of loss (in conductors and the ferrite core). However, its dependence on X_7, which is almost constant with frequency, is related to eddy current losses in the ferrite core, which normally should decrease with frequency.

One can clearly notice that the R parameter is strongly influenced by material uncertainties, including the material properties of conductors and the ferrite core.

5. Conclusions

In this chapter, we carried out a sensitivity analysis of RL parameters of a wound inductor according to the considered random inputs in our study. To deal with the

high dimension of the random input vector, we transformed geometrical uncertainties (linked to the positions of conductors in the winding window) into material ones, and we computed a surrogate model based on PCE across the wide range of frequencies in the study. This approach allowed us to compute *Sobol* indices related to the sensitivity analysis of output parameters with respect to the new random input vector, whose dimension has been reduced to seven. Our case study was conducted on a specific wound inductor (MCSCH895-680KU) to obtain reference values for computed output parameters from the numerical model used. Based on the sensitivity analysis, we found that the L parameter is mostly influenced by geometrical uncertainties (positions of conductors in the winding area), while the R parameter is mostly influenced by material uncertainties linked to the electrical and magnetic properties of conductors (electrical conductivity) and the ferrite core (magnetic permeability and electrical conductivity). Looking ahead, in the case of a non-symmetrical inductor geometry, it could be challenging to model in 3D the geometric uncertainties associated with the winding and to study their influence on the local electromagnetic behavior via the C parameter.

Appendices

Appendix A: Different strategies for PCE building

The PCE is the development $\mathcal{M}^{PC}(X)$ of a model response $Y = \mathcal{M}(X)$ in the space of random functions relating to the distributions of its random inputs X.

$$Y = \mathcal{M}(X) \approx \mathcal{M}^{PC}(X) = \sum_{\alpha \in \mathcal{A}} y_\alpha \varphi_\alpha(X), \tag{8}$$

where $\mathcal{A}$ is the truncated set of multi-indices of the PCE.

The computation of its coefficients y_α is carried out by different methods, including the most classic projection method [3], which uses multiple integrals. The number N of integration nodes depends on the dimension M of the random input and on the maximum degree p of the PCE according to the expression:

$$N = (p+1)^M \tag{9}$$

Hence, this explosion in the number of evaluations of the numerical reference model is often called the *curse of dimensionality*.

To build the PCE substitute, we start with a sample of size N of the random inputs (called the experimental design). The determination of the PCE coefficients then involves solving the following optimization problem:

$$\hat{y} = arg\ min\ \mathbb{E}\Big(y^T \varphi(X) - \mathrm{M}(X)\Big)^2, \tag{10}$$

For which the solution is given by the ordinary least squares (OLS) method, namely.

$$\hat{y} = (A^T A)^{-1} A^T y, \tag{11}$$

where $A_{ij} = \varphi(X)_j(x^{(i)})$ contains the values taken by the polynomial basis at the level of points of the experimental design and is called the experimental matrix $i = 1, \cdots, N; j = 0, \cdots, P-1$.

An important parameter for evaluating the quality of the constructed PCE is the relative empirical error, deduced from the experimental design. This kind of parameter can lead to over-fitting, since it decreases with the degree p of the PCE regardless of the size N of the experimental design. In order to overcome this problem, an adaptive

technique for constructing sparse PCEs using an *a priori* cross-validation error was used in this work. This type of PCEs implies low-order interactions between the random variables, which are, by experience, the most important in various numerical models (sparsity-of-effects principle). This was taken into account in the initial optimization problem (see Equation [6]) by associating it with a penalty term of the form $\lambda||y||_1$, that is, the problem:

$$\hat{y} = arg\ min_{y\in\mathbb{R}^{|\mathcal{A}|^n}}\ \mathbb{E}[(y^T\varphi(X) - \mathcal{M}(X))^2] + \lambda||y||_1, \tag{12}$$

where the regularization term $|\hat{y}||_1 = \sum_{\alpha\in\mathcal{A}}|y|_\alpha$ forces the minimization to favor low-rank solutions. In this latter context, the least angle regression (LAR) algorithm is the one implemented in UQLab [14], a specific module for uncertainty quantification under MATLAB.

From **Table A1**, we can observe the accuracy with which we manage to fit the parameter R (from the FE method) at 1.2 MHz, thanks to the LAR strategy. For the same maximum degree, one observes a sparser basis than with the OLS strategy.

$R_{@1.2\text{MHz}}$ [Ω]	Error	Max. degree	Non-zero coefficient.
OLS	0.4723	2	15
LAR	0.0406	2	8

Table A1.
Comparing OLS and LAR strategies for the surrogate model of $\mathrm{R}_{@1.2\text{MHz}}$ *parameter.*

Author details

Geoffrey Lossa[1,2*] and Olivier Deblecker[2]

1 ISPT-Kinshasa, Kinshasa, DR Congo

2 University of Mons, Mons, Belgium

*Address all correspondence to: glossa@isptkin.ac.cd

References

[1] Lossa G, Deblecker O, De Grève Z. Influence of geometric uncertainties on the RL parameters of wound inductors modelled using the finite element method. IEEE Transactions on Magnetics Miami. 2017;**53**(6)

[2] Sudret B.Global sensitivity analysis using polynomial chaos expansionexpansions. Reliability Engineering and System Safety. 2008;**93** (7):964–979

[3] Marelli S, Luthen N, Sudret B. Polynomial chaos expansions - UQLab user manual. In Chair of Risk, Safety and Uncertainty Quantification. ETH Zurich, Switzerland; 2022

[4] Otto F, Gloria A, Duerinckx M, Characterization of fluctuations in stochastic homogenization, Workshop on Uncertainties Quantification, 3rd GAMM AGUQ, 2018

[5] Meunier G, et al. Homogenization for periodical electromagnetic structure: Which formulation? IEEE Transactions on Magnetics 2010;**46**:3409–3412

[6] Vazquez Sabriego R, et al. Time-domain homogenization of windings in 3-D finite element models. IEEE Transactions on Magnetics 2008;**44**:3989–3991

[7] Lossa G, Deblecker O, De Grève Z, Comparing Two Approaches for Generating Realistic Patterns in the 2D Stochastic FE Modeling of Wound Inductors, 2020. Available from: https://www.researchgate.net/publication/343335404ComparingtwoApproachesforGeneratingRealisticPatternsinthe2DStochasticFEModelingofWoundInductors

[8] Lossa G, Deblecker O, Geuzaine C, De Grève Z, Building fast stochastic surrogate models for extraction of RL parameters of wound inductors modelled using FEM, IEEE Xplore, CEFC 2021, Pisa

[9] Wagner P-R, Nagel J, Marelli S, Sudret B. Bayesian Inference for Model Calibration and Inverse Problems - UQLab User Manual. ETH Zurich, Switzerland: Chair of Risk, Safety and Uncertainty Quantification; 2022

[10] Marelli S, Sudret B, UQLab: A framework for uncertainty quantification in Matlab, Int. Conf. on Vulnerability, Risk analysis and Management, Proc. 2nd ICVRAM, Liverpool, UK, 2014, 2554–2563

[11] Lossa G, Deblecker O, De Grève Z, Experimental Validation of Geometrical and Material Uncertainties Consideration in the Modeling of Wound Inductors Using FEM. In: Photonics & Electromagnetics Research Symposium (PIERS); 2021; Hangzhou, China. p. 69–73. DOI: 10.1109/PIERS53385.2021.9694904

[12] Geuzaine C, Remacle J-F.Gmsh: A three-dimensional 3-D finite element mesh generator with built-in pre- and post-processing facilities. International Journal for Numerical Methods in Engineering. 2009;**79** (11):1309–1331

[13] Lossa G, Deblecker O, De Grève Z. Influence of material uncertainties on the RLC parameters of wound inductors modeled using the Finite element method. Open Physics. 2018;**16**(1): 227–231

[14] Marelli S, Sudret B, UQLab user manuel – Polynomial chaos expansions, Chair of Risk, Safety and Uncertainty Quantification, Report # UQLab-V1.3-104, ETH Zurich, Switzerland, 2019